Available online at www.sciencedirect.com
ScienceDirect
Medical Engineering & Physics 31 (2009) 145–152
Medical Engineering & Physics
www.elsevier.com/locate/medengphy

Mathematical model to simulate the extracellular myoelectrical activity of the cat colon

N. Mirizzi [a,*], M.A. Strangio [b], R. Mirizzi [c], G. Riezzo [d]

[a] *Department of Physics, University of Bari, Italy*
[b] *Department of Mathematics, University of Rome "Roma Tre", Italy*
[c] *Polytechnic of Bari, Italy*
[d] *Laboratory of Experimental Pathophysiology "S. de Bellis", National Institute for Digestive Diseases, Castellana Grotte (BA), Italy*

Received 10 September 2007; received in revised form 10 April 2008; accepted 16 April 2008

Abstract

The rationale of this study was to investigate if the bases of generation of the electrical activity of the whole gut are the same. For this reason, we developed a mathematical dipole model, based on the same foundations used to simulate the electrical activity of the human stomach, to generate the electrical activity of the transverse cat colon. The model developed takes into account both the geometry of the transverse colon represented by a cylinder of finite length and the myoelectrical dynamics of the cells. The extracellular electrical activity was simulated by the periodic movement of an annular band polarised by electric dipoles. The simulation not only reproduces both the waveform, amplitude, phase lag and frequency of the ECA and the frequency, duration and periodicity of the ERA but also allows us to reproduce both increases/decreases of frequency, the inversion of phase conditions of the ECA and ERA, and to underline the anatomical and physiological parameters that can modify the ECA amplitude, such as the radius of the colon and the cells' dipole moment density. The simulation also picks up not only the effects of the probes' type (unipolar, bipolar, endoluminal, external) and of their positioning during *in vivo* experiments made by implanted electrodes to record the ECA and ERA, but also allows us to find both the theoretical best configuration for the surface electrodes and the effects of the distance between the abdominal electrodes and the source of the electrical activity, and of the distance between the electrodes.

Keywords: Cat colon; Computer simulation; Extracellular electrical activity; ECA; ERA

1. Introduction

The electrical activity of the gastrointestinal tract (GI) consists of electrical control activity (ECA, slow waves) and electrical response activity (ERA, spike bursts). As reported by several experimental studies, slow waves are generated from the complex electrochemical interaction between the smooth muscle cells and specialised cells called interstitial cells of Cajal (ICC), and both realise the fundamental components of the myogenic control system (MCS). The ICC cells are the pacemaker of the gut [1] and generate pacemaker potentials that produce rhythmical depolarisation of the membrane [2,3]. The ECA activity controls the occurrence of contractions in the time and space. The ERA is made up of two components: plateau and spikes. Several authors [4,5] have related that the spikes are superimposed over the plateau of the ERA and that its occurrence is started by the injection of Ca^{2+} ions into the smooth muscle cells. It is also known that the ERA spike bursts are the trigger for the contractions.

Many models have been developed to simulate the electrical activity of the GI tract. Generally, these models are divided into three categories: relaxation oscillators models [6–9], volume-conductor models [10–12] and dipole-based models [13–15]. The question to establish which category of models is the most appropriate has been the subject of a great deal of debate, but the consensus appears to be that each of the different types of model reveals specific features of the GI electrical activity [16,17].

* Corresponding author. Tel.: +39 0805442417; fax: +39 0805442434.
E-mail address: nicola.mirizzi@ba.infn.it (N. Mirizzi).

1350-4533/$ – see front matter © 2008 IPEM. Published by Elsevier Ltd. All rights reserved.
doi:10.1016/j.medengphy.2008.04.016

To verify the achievability of the rationale, we developed an electric dipole-based mathematical model that reproduces the myoelectrical activity of the cat colon, taking into account its geometrical characteristics and the myoelectrical dynamics of the cells. To validate the model: (a) the most significant characteristics of the ECA and ERA were simulated; (b) the effects of the probes' type (implanted and abdominal surface electrodes) and configuration (unipolar/bipolar electrodes) on the quality of the ECA recordings were studied; and (c) a continuous increase/decrease of the frequency and a phase inversion of the ECA were simulated.

2. Mathematical model

To take into account the cat colon anatomy and the myoelectrical dynamics of the cells, the mathematical model was developed under the following conditions:

- The colon was represented by a set of three cylinders (one for each segment) of fixed length, with a constant section. As reported in the literature [18,19], the cat colon is a tubular structure mainly composed of the serosa, the longitudinal muscular layer, the ICC-MY, the circular muscular layer, the ICC-SMP and the mucosa (Fig. 1(a)).
- The cells were represented as electric dipoles. In fact, it is known that the GI smooth muscle cells have a *resting membrane potential* (RMP) due to a balanced ionic distribution across the cells' membrane. Such distribution causes the internal side of the cellular membrane to be negative and the external positive. The pacemaker potentials generated by the interstitial cells of Cajal [1,3] upset the balance and cause the inversion of polarity across the cells' membrane by a periodic membrane depolarisation.
- The cells that, at a given instant, gave rise to the membrane depolarisation were spread in an annular band δ-wide belonging to the cylinder. Fig. 1(b) is a schematic representation of an element of the annular band δ-wide polarised by electric dipoles perpendicularly oriented to the surface of the cylinder.
- The distribution of the dipoles in the remaining part of the cylinder was random so that it generated a null potential in each and every point of the space.
- The moment dipole density $\boldsymbol{D}$ of the polarised annular band was taken as constant.
- The electrical permittivity of the abdominal wall was taken as constant and equal to $\varepsilon = \varepsilon_0\varepsilon_r$ (ε_0 is the electrical permittivity in free space; ε_r is the mean value of the relative electrical permittivity of the abdominal wall layers (muscle, fat, skin, etc.) in the frequency range 1 to 10 Hz). Appendix C of [20] reports the diagrams showing the properties of many body tissues in the frequency range from 1.0E+1 to 1.0E+11 Hz.

Under the conditions set, the potential generated by the annular band δ-wide, in each and every point of the space, was valued by means of the following integral (see Appendix A for the mathematical details):

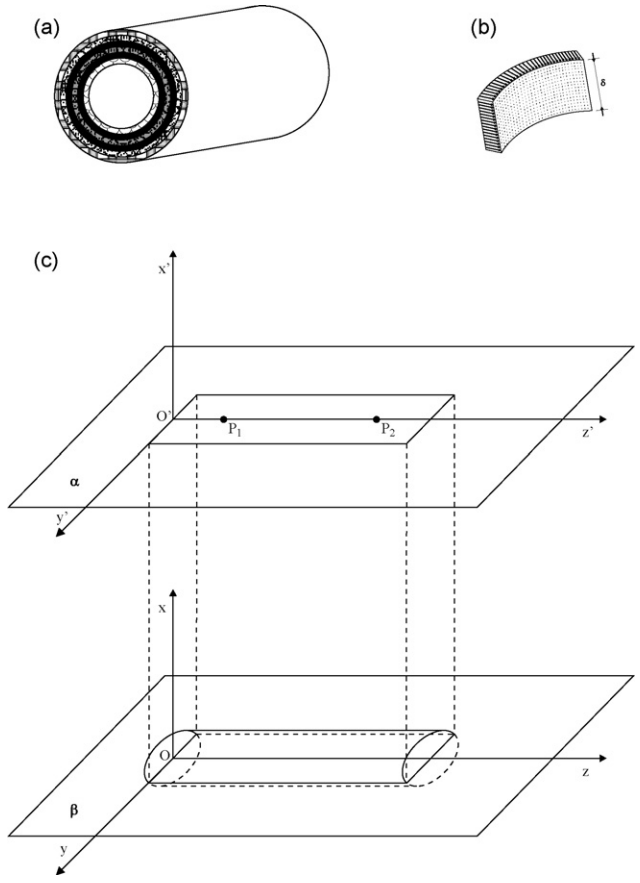

Fig. 1. (a) The traverse colon is represented by six concentric cylinders that, going from the outer to the inner, represent the serosa, the longitudinal muscular layer, the ICC-MY, the circular muscular layer, the ICC-SMP and the mucosa. In (b) an element of the circular muscular layer with polarised cells is represented. In (c) the geometrical representation of the cylinder represents the colon on the abdominal surface. The plane α represents the abdominal surface.

$$V(\mathbf{r},t) = \frac{-D}{4\pi\varepsilon}\int_0^{2\pi}\int_{z(t)}^{z(t)+\delta} \times \frac{R_0 z[R_0 - h\cos(\Theta-\theta)]\mathrm{d}z\mathrm{d}\Theta}{\{z^2+z_P^2+R_0^2+h^2-2[zz_P+R_0h\cos(\Theta-\theta)]\}^{3/2}(R_0^2+z^2)^{1/2}}. \quad (1)$$

3. Simulation of colonic electrical activities

The computer simulation was based on the specific electrophysiogical characteristics reported above. The membrane depolarisation, after its initiation, propagates as a wave into the adjacent muscle layers [21] at a constant velocity and gives rise to the omnipresent cyclical slow waves. The main characteristics of the electrical activity of the cat colon are widely reported in the literature [22,23] (see Table 1). As regards the ECA frequency of the cat colon, there are different opinions. In fact, Christensen et al. [24] said that slow waves of the proximal colon were rather irregular at 1–4 cpm; those in the distal colon were more regular at 5–7 cpm. In this

Table 1
Main anatomical and physiological characteristics of the cat colon

Parameters	Values
Anatomical	
Length	From 0.20 to 0.40 m
Diameter (depending on the size of the cat)	From 0.025 to 0.030 m
Physiological	
ECA pattern *in vivo* [22]	
Frequency	
Ascending colon	5.3 ± 0.4 cpm
Transverse colon	5.4 ± 0.4 cpm
Descending colon	5.5 ± 0.5 cpm
Amplitude [23]	Up to 1.5 mV
ERA patterns *in vivo* [22]	
Short spike burst (phase-locked to slow waves)	
Frequency	Up to 10 Hz
Duration	Up to 5–6 s
Long spike burst (not phase-locked to slow waves)	
Frequency	Up to 10 Hz
Duration	Up to 30 s
Recurrence	0.7–1.5 min

paper, we simulated the extracellular electrical activity of the transverse tract of the cat colon: ECA, the long spike burst, and the short spike burst as described in [22]. However, the model is also valid for the other tracts of the colon and can simulate any frequency.

The circular muscular layer where the ECA is generated [22] was simulated by a cylindrical surface. In the simulation, the annular band moved from the top to the bottom of the transverse segment.

To simulate the ECA by Eq. (1) it was assumed that:

- It was generated by a periodic movement of the δ-wide annular band along the whole length of the cylinder from one end to the other and then back again.
- The movement of the annular band was paced by the intrinsic pacemaker belonging to the selected segment.
- The band moved according to the law:

$$z = v \cdot t.$$

For every segment, the velocity v of the annular band was taken as constant and dependent on the ECA period T.

For a segment of length l, the velocity v was determined by the following relationship:

$$v = \frac{l}{T} = l \cdot f,$$

where f is the frequency (measured in Hz) of the ECA of a given segment.

Since the exact length of each segment was not available in the literature, we assumed that the length of the ascending tract was 8 cm, that of the transverse tract 10 cm and that of the descending tract 12 cm. The main values of the factors set to simulate the morphological characteristics of the ECA (waveform, amplitude, frequency) in our study are reported in Table 2. To simulate the electrical activity recorded by electrodes implanted in the muscular layer of the colon, we took $\varepsilon = 2.65625\text{E}{-4}\ \text{C}^2/(\text{N m}^2)$. To simulate the electrical activity recorded by external electrodes, we took $\varepsilon = 2.213545625\text{E}{-4}\ \text{C}^2/(\text{N m}^2)$. This value was obtained by multiplying ε_0 by the mean value of the relative permittivity ε_r of the muscle and fat layer of the abdominal wall.

To study the effects of the probes' type on the colonic electrical activity, implanted unipolar and bipolar, intraluminal and external probes were simulated. The unipolar implanted probes were simulated by calculating as the electrical potential in a point of the cylinder surface varied over the time. The bipolar implanted and endoluminal probe were simulated by calculating as the electrical potential difference between two points, 0.002 m apart, varied over the time.

To simulate the ECA recorded by an abdominal probe (see Fig. 1(c)):

- the abdominal surface was represented by means of a plane α;
- the cylinder representing the colon was cut by means of a plane β parallel to the plane α. The cylinder axis was taken coincident with the z axis of the $Oxyz$ system;
- the cylinder cross-section lying in the plane β was projected on the plane α;
- the $O'x'y'z'$ system was drawn in the plane α. The axis z' was taken coincident with the axis of the cylinder cross-section on the α plane;
- the two planes were supposed to be separated by a dielectric of permittivity ε.

The electrical potential difference was calculated between the two points P_1 and P_2 positioned on the z'. The distance between the two points P_1 and P_2 was taken to be equal to 4 cm. The distance between the two axes z' and z was taken to be equal to 6.125 cm.

Illustrative examples of the colonic electrical activity are given in Figs. 2–8. Both a continuous decreased rhythm and an inversion of phase are evident in the ECA plotted in Fig. 2, obtained by simulating unipolar implanted electrodes. However, with the model here proposed it is also possible to simulate a transient frequency and phase uncoupling. To simulate the frequency decrease, the velocity of the annular band was decreased. To simulate the inversion of phase, the annular band moved from the bottom to the top of the colon. A con-

Table 2
Values of the parameters used to simulate colonic ECA

Parameters	Values
Frequency	5.4 cycle/min
Amplitude	1.5 mV
Cylinder length	0.10 m (transverse colon)
Cylinder radius, R_0	0.0125 m
Dipole moment p of annular band	0.45×10^{-9} C × m
Annular band width, δ	0.00011 m
Permittivity, ε_0	$8.85418\text{E}{-12}\ \text{C}^2/(\text{N m}^2)$
Colon relative permittivity, ε_r	2.5E+7
Muscle relative permittivity, ε_r	4.0E+7
Fat relative permittivity, ε_r	1.0E+7

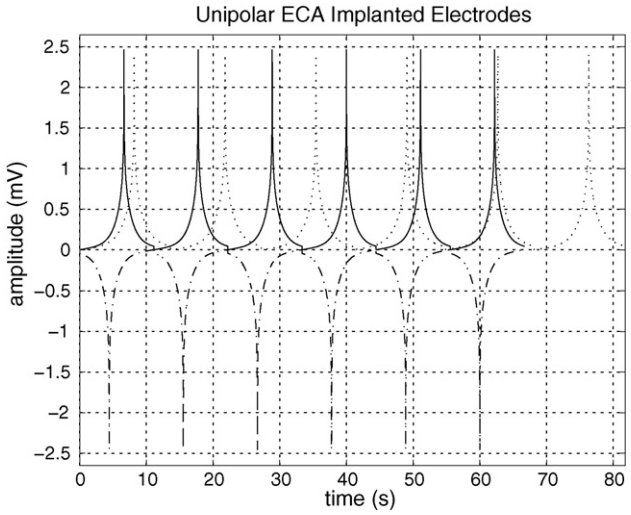

Fig. 2. ECA obtained by simulating the extracellular unipolar electrode implanted in the muscular layer. The plot in the solid line simulates the ECA with the normal frequency of 5.4 cpm; the plot in the dotted line simulates the ECA with a frequency of 4.4 cpm. For both the plots, the annular band moves from the top to the bottom of the transverse colon; the plot in the dash-dot line simulates the ECA with a frequency of 5.4 cpm. The annular band moves from the bottom to the top of the transverse colon. For all the plots, the rectangular coordinates where the electrode was implanted are $(R_0/\sqrt{2}, R_0/\sqrt{2}, 0.06)$.

tinuous phase lag and a distal amplitude gradient are evident in the ECA plotted in Fig. 3, obtained by simulating bipolar electrodes implanted at two different sites. A different waveform and amplitude with respect to the plots reported in Fig. 2 are also evident.

A difference in the ECA amplitude and waveform is evident between Figs. 4 and 5, obtained by simulating endoluminal and external probes, respectively.

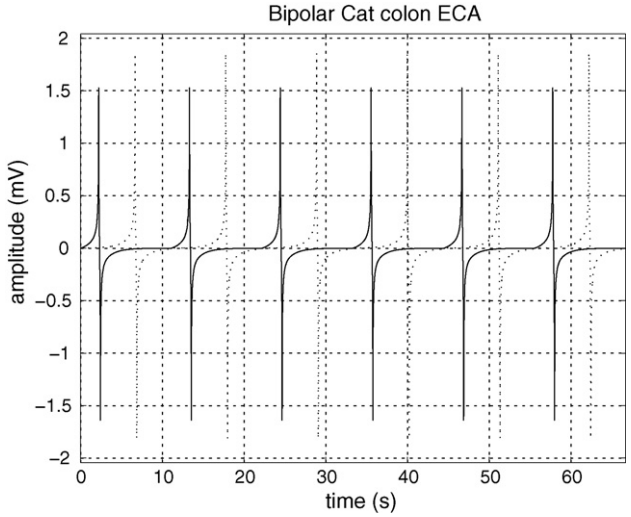

Fig. 3. ECA obtained by simulating extracellular bipolar electrodes implanted in the muscular layer. The signal in the solid line is relative to the points of coordinates $(R_0/\sqrt{2}, R_0/\sqrt{2}, 0.08)$ and $(R_0/\sqrt{2}, R_0/\sqrt{2}, 0.082)$, respectively; that in the dotted line is relative to the points of coordinates $(R_0/\sqrt{2}, R_0/\sqrt{2}, 0.04)$ and $(R_0/\sqrt{2}, R_0/\sqrt{2}, 0.042)$, respectively. Observe the change in amplitude in the signals plotted at the two different sites.

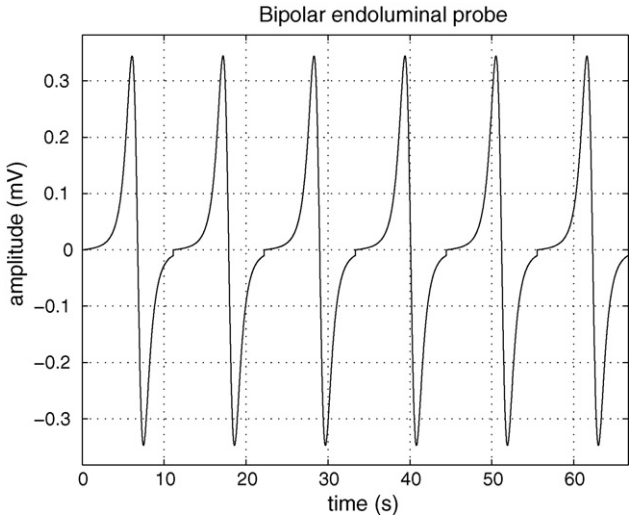

Fig. 4. ECA obtained by simulating an endoluminal probe. The signal was obtained by calculating the electrical potential difference between the points of coordinates (0, 0 and 0.04) and (0, 0 and 0.042), respectively.

A difference in the ECA amplitude for different values of the cylinder radius is observed in Fig. 6, obtained by simulating extracellular bipolar implanted probes. The dipole moment p was taken as equal to 0.45×10^{-9} C × m.

A difference in the ECA amplitude for different values of the dipole moment p is observed in Fig. 7, obtained by simulating extracellular bipolar implanted probes. The radius R_0 of the cylinder was taken as equal to 0.0125 m.

In [22] it is reported that: (a) the ERA occurs in a burst; (b) the spike frequency in the burst is higher than that of the ECA; (c) the spike amplitude in the burst is less than that of the ECA and is not constant; and (d) there is a phase relation between the ECA and the ERA. Since in our model the frequency of the electrical activity depends on the velocity of the annular band, we increased the speed of the annular

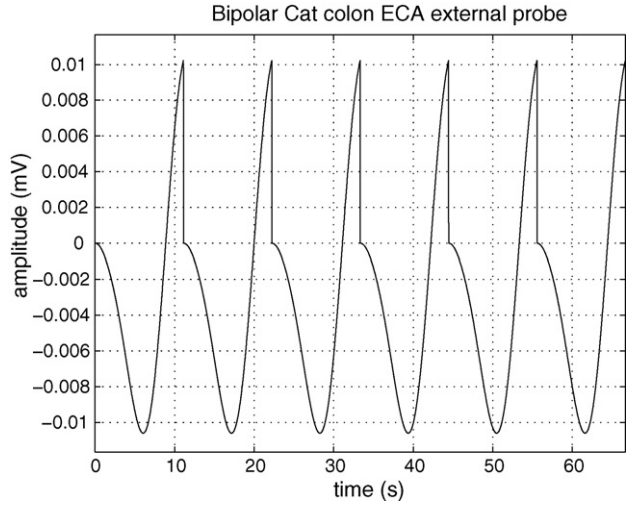

Fig. 5. ECA obtained by simulating bipolar electrodes external to the cylinder in the points of coordinates (0.06125, 0 and 0.04) and (0.06125, 0 and 0.08), respectively. The distance between the two points is equal to 0.04 m.

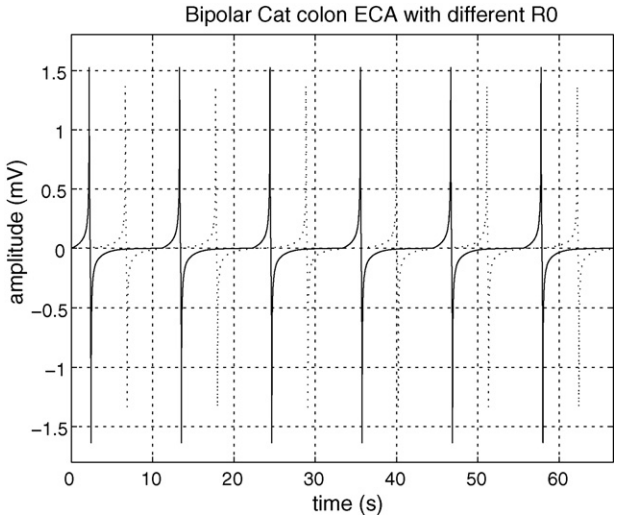

Fig. 6. ECA obtained by simulating extracellular bipolar electrodes implanted in the muscular layer for two different values of the cylinder radius: solid line ($R_0 = 0.0125$ m), dotted line ($R_0 = 0.0145$ m).

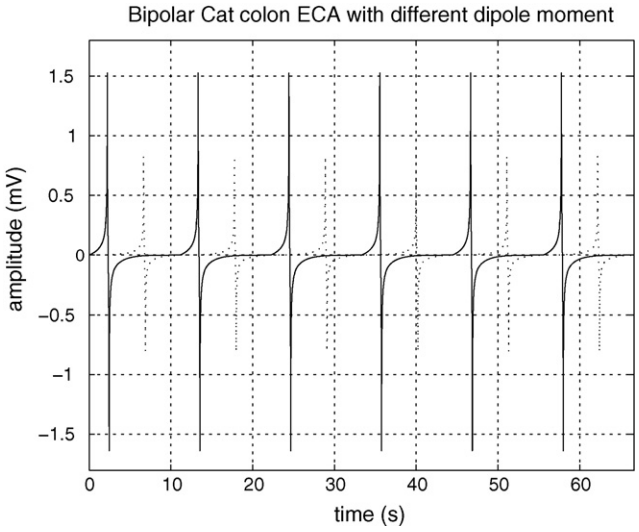

Fig. 7. ECA obtained by simulating extracellular bipolar electrodes implanted in the muscular layer for two different values of the dipole moment p: solid line $p = 0.45 \times 10^{-9}$ C × m, dotted line $p = 0.2 \times 10^{-9}$ C × m.

band to simulate the spike frequency during the ERA burst. It is known that the ERA amplitude is not constant over time, so it was simulated randomly as variable. The main parameters' values set to simulate the morphological characteristics of the ERA are reported in Table 3. The ERA characteristics were simulated by fixing: (a) the time when a burst occurs to establish its phase in respect of the ECA; (b) the spike frequency in the burst; (c) the maximum amplitude of the spikes in the bursts; (d) the duration of the bursts and their periodicity, if present; and (e) the direction of propagation of the spikes. A short burst ERA is shown in Fig. 8(a), and the simultaneous presence of the ECA, a short burst ERA and a long burst ERA are shown in Fig. 8(b). They were obtained by simulating a bipolar configuration of probes positioned in the points with rectangular coordinates (R_0, 0 and 0.08 m) and (R_0, 0 and 0.082 m).

Table 3
Values of the parameters used to simulate colonic ERA

Parameters	Values
Frequency	5 Hz up to 10 Hz
Amplitude	Random, up to 1 mV
Short burst duration	2 s
Long burst duration	16 s
Cylinder length	0.10 m
Cylinder radius, R_0	0.0125 m
Dipole moment, p	0.3×10^{-9} C × m
Annular band width, δ	0.00011 m
Permittivity, ε_0	8.85418E−12 $C^2/(N\,m^2)$
Colon relative permittivity, ε_r	2.5E+7
Muscle relative permittivity, ε_r	4.0E+7
Fat relative permittivity, ε_r	3.0E+7

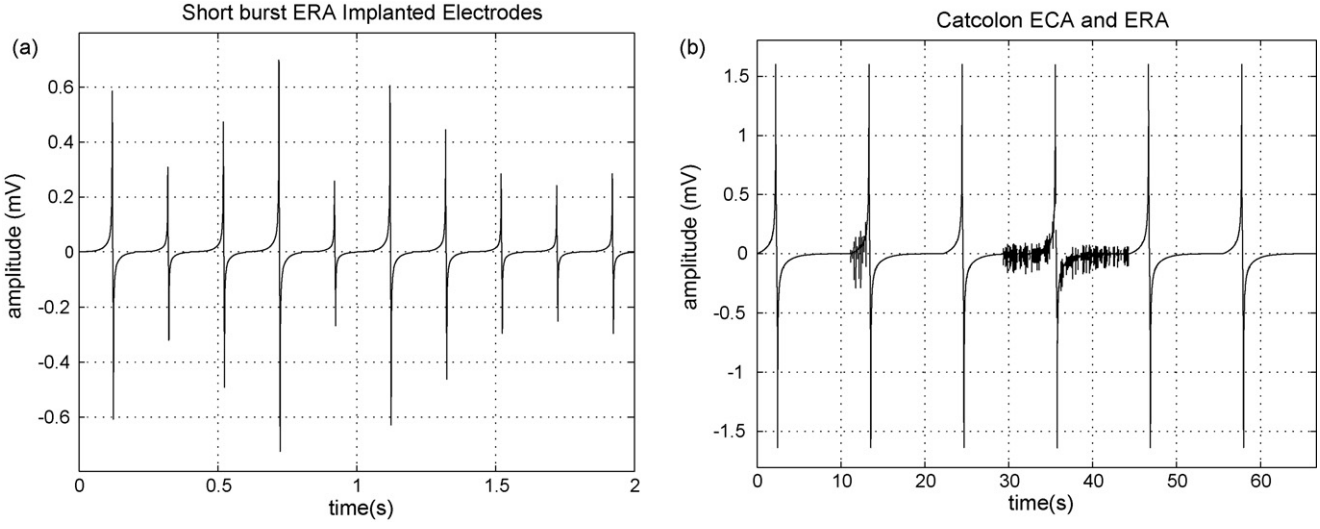

Fig. 8. (a) Short burst ERA; (b) signal composed by the ECA, a short burst ERA, phase lock to the ECA and a long burst ERA.

4. Discussion

The computer simulation of the colonic electrical activity provides concrete evidence that our model accurately reproduces the characteristics of the cat colon ECA (waveform, amplitude, frequency and phase lag) and ERA (short burst, long burst) as reported *in vivo* by Wienbeck [22]. This is a remarkable achievement that confirms the validity of the dipole-based model and proves that the simulation parameters were appropriately chosen. An appealing property of the model is its flexibility and the advantage of being easily simulated by computer.

For a given radius R_0, the ECA amplitude can be changed by varying the dipole moment p. A modification of dipole moment p is related to the number of the cells which depolarise–polarise simultaneously in the annular band. However, since the colon is not a rigid tube (the radius R_0 of the cylinder can change and consequently the amplitude can also change), the amplitude also depends on the radius R_0 of the cylinder. Therefore, we believe that the amplitude, taken by itself, is not a reliable parameter to discriminate normal from pathological conditions.

Also, the effects of the implanted probes' type, configuration and position were clearly indicated from the results obtained. In fact, a difference in the ECA amplitude was observed by simulating unipolar and bipolar probes implanted in the muscular layer. In particular, the bipolar recordings show a lower amplitude but they are more convenient as they allow an input differential amplifier, that rejects the unwanted common mode signals, to be used. In agreement with [25] and [26], the simulation provides evidence that the ECA amplitude depends on the distance between the electrical signals' source and the probe. We think that this fact may explain the different amplitude values found comparing several *in vitro* and *in vivo* experiments and suggests that to make the ECA amplitude comparable it is important to standardise the probe positioning when performing *in vivo* recordings with implanted probes. Besides, the simulation provides evidence that the ECA amplitude also depends on the distance between the electrodes.

When external bipolar probes were simulated, we noted that the amplitude of the electrical activity was closely dependent on the distance between the bipolar electrodes, on the distance between the electrodes and the source of the electrical signal, and on the direction of the axis joining the two electrodes with respect to the z' axis. The simulation of external bipolar probes underlined that the ECA vanished when the electrodes of the abdominal bipolar probe were positioned symmetrically on an axis perpendicular to the z' axis and reached a maximum when the electrodes were positioned on an axis parallel to the colon axis traced on the intersection of the abdominal surface with the orthogonal plane containing the colon axis (the z' axis of Fig. 1(c)). Mirizzi and Scafoglieri [27] experimentally verified that to optimise the amplitude of the human stomach ECA, recorded from the abdominal surface, the electrodes have to be positioned on an axis parallel to the antral axis. This configuration allows the clinical use of the cutaneous electrogastrography (EGG). So, we believe that all these results indicate that the model proposed may be used to improve the *in vivo* recordings technique with implanted and abdominal probes. The simulation of the abdominal bipolar probe reproduces exactly the ECA frequency. We cannot say whether the simulation also exactly reproduces the morphology of the ECA waveform since in the literature there are no *in vivo* recordings made from the abdominal surface of the cat. Besides, the model has some limitations regarding the electrical activity recorded from external electrodes (see below).

When the ERA was simulated with the model proposed here, it was possible to change all the ERA characteristics we simulated, that is: (a) the time when a burst occurs and hence the phase in respect of the ECA; (b) the spike frequency in a burst; (c) the spike amplitude; (d) the duration of the spike bursts and their periodicity, if present; (e) the direction of propagation of the spikes (see Fig. 8(b)). Since there is a large decrease in the ECA amplitude obtained by simulating an external probe, to record the ERA it is necessary to use an amplifier with a gain much greater than the one used to record the ECA.

The limitations of the model are included in the following considerations: (a) it neglects the inhomogeneities of the abdominal wall. We neglected the inhomogeneities of different layers because the assumption of homogeneity greatly simplifies the modelling. The abdominal wall was considered as homogeneous in most models; (b) it does not consider the effects due to the contact of the electrodes to the skin; (c) it does not take into account the electrodes' dimensions; (d) it does not take into account the external noise on the abdominal surface due to other internal organs; and (e) it does not take into account the effects of the amplifier band. Besides, when external bipolar probes were simulated, we noted that the ECA morphology depends on the electrodes' configuration (electrodes' distance and position with regard to the z' axis). All these limitations and conditions surely make the waveform of the electrical activity, recorded from the abdominal surface with *in vivo* experiments, different from that obtained by simulation. Another limitation of the model is the fact that the cylindrical geometry is a schematic representation of the real colon.

Anyway, the model offers the possibility to simulate the most significant characteristics of the electrical activity accurately enough, including some specific patterns such as frequency variation and phase inversion. In addition, it allows us to study the effects of the probes' type and configuration on the quality of the ECA recordings.

5. Conclusion

The results obtained from the simulation of the electrical activity of the cat colon clearly show that the objective was reached: (a) the most significant characteristics of the ECA

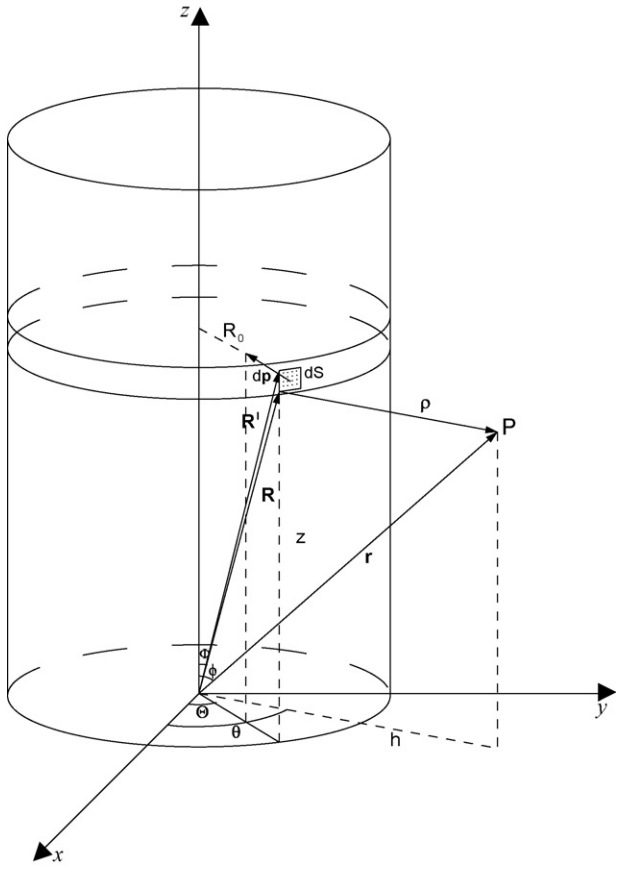

Fig. 9. Geometric arrangement of the vectors **r**, **R**, **ρ**, d**p**.

and ERA were simulated; (b) the effects of the probes' type (implanted unipolar/bipolar electrodes) and configuration (abdominal surface electrodes) on the quality of the ECA recordings were studied; (c) a continuous increase/decrease of the frequency and phase inversion of the ECA was simulated.

The next developments will concern the other phenomena that can be simulated with a dipole-based model, considering both implanted and external electrodes.

Appendix A

The cylinder in Fig. 9 is a schematic representation of the transverse tract of the cat colon. Indicating the dipole moment of the infinitesimal area dS by $\boldsymbol{p}$ and the dipole density of the annular polarised band by $\boldsymbol{D}$, the potential dV generated at the generic point P in the space, using the dipole approximation, is:

$$\mathrm{d}V = \frac{1}{4\pi\varepsilon}\frac{\boldsymbol{\rho}\cdot\mathbf{D}}{\boldsymbol{\rho}^3}\mathrm{d}S,$$

where $\boldsymbol{\rho}$ is the vector joining the surface element dS with the point P (Fig. 9) and $\boldsymbol{D}$ is the dipole moment density of the annular band. Hence,

$$V(\mathbf{r}) = \frac{1}{4\pi\varepsilon}\iint_S \frac{\boldsymbol{\rho}\cdot\mathbf{D}}{\boldsymbol{\rho}^3}\mathrm{d}S,$$

with $\mathbf{D}\mathrm{d}S = \mathrm{d}\mathbf{p}$.

From Fig. 9, it follows that $\boldsymbol{\rho} = \mathbf{r} - \mathbf{R}$; expressing the components of $\boldsymbol{\rho}$ we have

$$\boldsymbol{\rho}\cdot\mathbf{D} = -D[R\sin\Phi - r\sin\phi\cos(\Theta-\theta)]$$

and

$$\boldsymbol{\rho} = \{R^2 = r^2 - 2Rr[\cos\Phi\cos\phi + \sin\Phi\ \ \sin\phi\cos(\Theta-\theta)]\}^{1/2}.$$

Since $\mathrm{d}S = R\sin\Phi\mathrm{d}\Theta\mathrm{d}R$ and $|\mathbf{R}' - \mathbf{R}| = \mathrm{d}R$, the following expression is obtained for $V(\mathbf{r})$:

$$V(\mathbf{r}) = \frac{-D}{4\pi\varepsilon}\int_0^{2\pi}\int_{R_1}^{R_2} \times \frac{[R\sin\Phi - r\cos(\Theta-\theta)\sin\phi]R\ \ \sin\Phi}{\{R^2 + r^2 - 2Rr[\cos\Phi\cos\phi + \sin\Phi\sin\phi\cos(\Theta-\theta)]\}^{3/2}}\mathrm{d}R\mathrm{d}\Theta.$$

From Fig. 9, if R_0 is the radius of the cylinder surface, z the position of dS with respect to the z axis and x_P, y_P, z_P are the rectangular coordinates of the point P, we have

$$R = \sqrt{R_0^2 + z^2} \quad \mathrm{d}R = \frac{z\mathrm{d}z}{\sqrt{R_0^2 + z^2}}.$$

So finally the function to integrate becomes

$$f(z,\Theta)\mathrm{d}z\mathrm{d}\Theta = \times \frac{-R_0 z[R_0 - h\cos(\Theta-\theta)]\mathrm{d}z\mathrm{d}\Theta}{\{z^2 + z_\mathrm{P}^2 + R_0^2 + h^2 - 2[zz_\mathrm{P} + R_0 h\cos(\Theta-\theta)]\}^{3/2}(R_0^2 + z^2)^{1/2}}$$

with

$$h = (x_\mathrm{P}^2 + y_\mathrm{P}^2)^{1/2}.$$

So, for $V(\mathbf{r})$, the following is obtained:

$$V(\mathbf{r}) = \frac{D}{4\pi\varepsilon}\int_0^{2\pi}\int_z^{z+\delta} f(z,\Theta)\mathrm{d}z\mathrm{d}\Theta.$$

Since the annular band moves along the cylinder surface, $z = z(t)$, then

$$V(\mathbf{r},t) = \frac{-D}{4\pi\varepsilon}\int_0^{2\pi}\int_{z(t)}^{z(t)+\delta} \times \frac{R_0 z[R_0 - h\cos(\Theta-\theta)]\mathrm{d}z\mathrm{d}\Theta}{\{z^2 + z_\mathrm{P}^2 + R_0^2 + h^2 - 2[zz_\mathrm{P} + R_0 h\cos(\Theta-\theta)]\}^{3/2}(R_0^2 + z^2)^{1/2}}.$$

Hence, by means of a double integration, it is possible to obtain $V(\mathbf{r},t)$ in each and every point P of the space, given R_0, $\boldsymbol{\Theta}$ and the rectangular coordinates x_P, y_P, z_P of the point P.

Conflict of interest

Regarding the attached manuscript "Mathematical Model to Simulate the Extracellular Myoelectrical Activity of the Cat Colon" by N. Mirizzi, M. Strangio, R. Mirizzi, G. Riezzo

we certify that a financial and personal relationships in any form do not exist with other people or organization that could inappropriately influence our work.

References

[1] Camborova P, Hubka P, Sulkova I, Hulin I. The pacemaker activity of interstitial cells of Cajal and gastric electrical activity. Physiol Res 2003;52:275–84.

[2] David G, Hirst S, Suzuky H. Involvement of interstitial cells of Cajal in the control of smooth muscle excitability. J Physiol 2006;576(PI 3):651–2.

[3] Sanders KM. A case for interstitial cells of Cajal as pacemakers and mediators of neurotransmission in the gastrointestinal tract. Gastroenterology 1996;111:492–515.

[4] Zenilman ME. Abnormalities of intestinal motility. Austin, Georgtown: R.G. Landes Company; 1992.

[5] Suzuky H, Kito Y, Hashitani H, Nakamura E. Factors modifying the frequency of spontaneous activity in gastric muscle. J Physiol 2006;576:667–74.

[6] Linkens DA, Datardina SP. Frequency entrainment of coupled Hodgkin-Huxley type oscillator for modelling gastrointestinal electrical activity. IEEE Trans Biomed Eng 1977;24:362–5.

[7] Linkens DA. Electronic modelling of slow waves and spike activity in intestinal tissue. IEEE Trans Biomed Eng 1980;27:351–7.

[8] Bardakjian BL, Sarna SK. A computer model of human colonic electrical control activity. IEEE Trans Biomed Eng 1980;27:193–202.

[9] Familoni BO, Abell TL, Bowes KL. A model of gastric electrical activity in health and disease. IEEE Trans Biomed Eng 1995;42:647–57.

[10] Liang JIE, Chen JDZ. What can be measured from surface electrogastrography computer simulation? Dig Dis Sci 1997;42:1331–4.

[11] Bradshaw LA, Richards WO, Wikswo Jr JP. Volume conductor effects on the spatial resolution of magnetic fields and electric potential from gastrointestinal electrical activity. Med Biol Eng Comp 2001;39:35–43.

[12] Buist ML, Cheng LK, Yassi R, Bradshaw LA, Richards WO, Pullan AJ. An anatomical model of the gastric system for producing bioelectric and biomagnetic fields. Physiol Meas 2004;25:849–61.

[13] Mirizzi N, Stella R, Scafoglieri U. A model of extracellular waveshape of the gastric electrical activity. Med Biol Eng Comp 1985;23: 33–7.

[14] Mirizzi N, Stella R, Scafoglieri U. Model to simulate the gastric electrical control and response activity on the stomach wall and on the abdominal surface. Med Biol Eng Comp 1986;24:157–63.

[15] Irimia A, Bradshaw LA. Theoretical ellipsoidal model of gastric electrical control activity propagation. Phys Rev E Stat Nonlin Soft Matter Phys 2003;68:051905.

[16] Publicover NG, Sanders KM. Are relaxation oscillators an appropriate model of gastrointestinal activity? Am J Physiol 1989;256:C265–74.

[17] Daniel EE, Bardakjian BL, Huizinga JD, Diamant NE. Relaxation oscillator and core conductor models are needed for understanding of GI electrical activity. Am J Phyiol 1994;266:G339–49.

[18] Sturgess CP, Canfield PJ, Gruffydd-Jones TD, Stokes CR. A gross and microsopical morphometric evaluation of feline large intestinal anatomy. J Comp Pathos 2001;124:255–64.

[19] Bruni AC, Zimmerl U. Anatomia degli animali domestici. F. Vallardi, Milano; 1992.

[20] Gabriel C, Gabriel S. Compilation of dielectric properties of body tissues at RF and microwave frequencies. London: King's College; 1996.

[21] Sarna SK, Otterson MF. Myoelectric and contractile activities. In: Schuster MM, editor. Atlas of gastrointestinal motility. Baltimore: Williams & Wilkins; 1993. p. 3–42.

[22] Wienbeck M. The electrical activity of the cat colon in vivo. Res Exp Med 1972;158:268–79.

[23] Duthie HL. Progress report, electrical activity of gastrointestinal smooth muscle. Gut 1974;15:669–81.

[24] Christensen J, Caprilli R, Lund GF. Electrical slow waves in circular muscle of cat colon. Am J Physiol 1969;217:771–6.

[25] Suzuky N, Prosser CL, Dahms V. Boundary cells between longitudinal and circular layers: essential for electrical slow waves in cat intestine. Am J Physiol 1986;250:G287–94.

[26] Mintchev MP, Bowes KL. Computer simulation of the effect of changing abdominal thickness on the electrogastrogram. Med Eng Phys 1998;20:177–81.

[27] Mirizzi N, Scafoglieri U. Optimal direction of the electrogastrographic signal in man. Med Biol Eng Comp 1983;21:385–9.